

The Mechanism of Magnetic Interactions in the Bulk Ferromagnet *para*-(Methylthio)Phenyl Nitronyl Nitroxide (YUJNEW): A First Principles, Bottom-Up, Theoretical Study

Mercè Deumal,^{*[a]} Michael J. Bearpark,^[b] Michael A. Robb,^[b] Yves Pontillon,^[c] and Juan J. Novoa^{*[a, d]}

Abstract: The mechanism of magnetic interactions in the bulk ferromagnet *para*-(methylthio)phenyl nitronyl nitroxide crystal (YUJNEW) has been theoretically reinvestigated, using only data from ab initio calculations and avoiding any a priori assumptions. We first calculate the microscopic magnetic interactions (J_{AB} exchange couplings) between all unique radical pairs in the crystal, and then generate the macroscopic magnetic properties from the energy levels of the corresponding Heisenberg Hamiltonian. We thus propose a first principles, bottom-up (i.e. micro-to-macro) approach that brings theory and experiment together. We have applied this strategy to study the magnet-

ism of YUJNEW using data from the previously reported 298 and 114 K crystal structures, and also data from a 10 K neutron diffraction structure fully reported in this work. The magnetic topology at 298 K is two-dimensional: noninteracting planes, with three different in-plane J_{AB} pair interactions (+0.24, +0.09, and -0.11 cm⁻¹) and one numerically negligible (+0.02 cm⁻¹) inter-plane J_{AB} interaction. In contrast, the magnetic topology at 114 and 10 K

is three-dimensional, with two non-negligible in-plane J_{AB} constants (+0.11 and +0.07 cm⁻¹ at 114 K; +0.22 and +0.07 cm⁻¹ at 10 K) and one inter-plane pair interaction (+0.07 cm⁻¹ at 114 K; +0.08 cm⁻¹ at 10 K). Although this three-dimensional magnetic topology is consistent with YUJNEW being a bulk ferromagnet, there is only a qualitative agreement between computed and experimental magnetic susceptibility $\chi T(T)$ data at 114 K. However, the experimental $\chi T(T)$ curve is quantitatively reproduced at 10 K. The heat capacity curve presents a peak at around 0.12 K, close to the estimated experimental peak (0.20 K).

Keywords: ab initio calculations • magnetic properties • organic molecular magnets • structure–activity relationships

Introduction

The study of properties that result from the presence of magnetic interactions in molecular crystals has been a sub-


ject of interest for many groups in recent years.^[1] However, despite the enormous progress in this field, the design of molecule-based magnets is still not feasible, due to a limited understanding of the dependence of the microscopic mag-

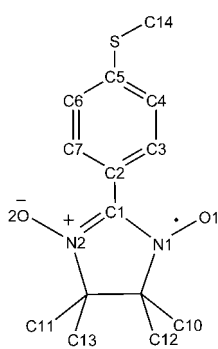
[a] Dr. M. Deumal, Prof. J. J. Novoa
Departament de Química Física, Universitat de Barcelona
Centre de Recerca en Química Teòrica (CeRQT)
Parc Científic de Barcelona
Av. Diagonal 647, 08028 Barcelona (Spain)
Fax: (+34)93-4021231
E-mail: m.deumal@qf.ub.es
novoa@qf.ub.es

[b] Dr. M. J. Bearpark, Prof. M. A. Robb
Chemistry Department, Imperial College London
South Kensington Campus, London SW7 2AZ (UK)

[c] Dr. Y. Pontillon
CEA—CEN de Cadarache, DEN/DEC/SA3C/LAMIR
13108 Saint Paul lez Durance (France)

[d] Prof. J. J. Novoa
Associate Member of the CEPBA-IBM Research Institute

 Supporting information for this article is available on the WWW under <http://www.chemeurj.org/> or from the author. Table S1: Theoretical (Mulliken) atomic spin populations calculated by means of DFT-UB3LYP/6-31+G(d) for an isolated *p*-(MeS)PhNN radical molecule in comparison with those determined experimentally. Figure S1: Convergence of computed $\chi T(T)$ data was checked at 298 K as the size of the magnetic model increases by propagating the minimal (1a,1c) model along *a* and *c* axes. Figure S2: Convergence of computed $\chi T(T)$ data was checked using J_{AB} values at 114 K by extending the minimal (1a,1c)₂ model along *a*, *b*, and *c* crystallographic axes. Figure S3: Convergence of computed $\chi T(T)$ data using J_{AB} values at 114 K as the size of the magnetic model increases by propagating the minimal (1a,1c)₂ model along *a*, *b*, and *c* axes. Figure S4: Simulated $\chi T(T)$ data using J_{AB} values at 298 K and model (1a,1c)₂ with interplane (*ac*) $J(d_6)$ values: 0, ± 0.02 and ± 0.07 cm⁻¹.



YUJNEW

Scheme 1. Structure of the *para*-(methylthio)phenyl nitronyl nitroxide radical.

netic interactions on the relative geometry of the interacting radicals and problems in predicting and controlling the packing of molecular solids.

To comprehend the magnetic properties of molecule-based magnets, it is essential to understand the reasons for the presence or absence of a given type of magnetic interaction. Such understanding can be gained by studying the mechanism of the magnetic interactions in crystals that have magnetic properties of special interest, such as the

small number of purely organic molecular magnets known to present bulk ferromagnetic behavior. One of these purely organic molecular ferromagnets is the *para*-(methylthio)phenyl nitronyl nitroxide crystal (radical hereafter identified as *p*-(MeS)PhNN, see Scheme 1,

$T_C=0.20$ K),^[2–5] whose magnetic interactions are the focus of this study.

The magnetic properties of the *p*-(MeS)PhNN crystal have been studied experimentally.^[2–5] There are crystal structures available at 298 K^[2] and 114 K,^[5] and a 10 K structure for which only the cell parameters have been previously published,^[4] and whose fractional coordinates are given in this work. No phase transition has been reported in the 10–298 K temperature range, and the only geometrical changes found are those due to thermal expansion. In such cases, the analysis of the magnetic interactions is very often done by using the room-temperature crystal structure, and the resulting conclusions are then extrapolated to any other low-temperature structure. In this work, we show that there are problems with this approach for *p*-(MeS)PhNN.

Two models of magnetic interaction have been proposed for the *p*-(MeS)PhNN crystal: one of interacting *ac* planes,^[2] with one in-plane and one inter-plane interaction, and a second model of noninteracting *ac* planes,^[3] with three different in-plane interactions. The second model was discarded on the basis of EPR data indicating the existence of magnetic interactions between the planes.^[2] When the first model was used to fit the magnetic susceptibility data, the best fit was obtained with fitting constants $J=+0.18$ K and $J'\cong+0.042$ K.^[3,6] These two models were selected on the basis of two empirical generalizations about the nature of the magnetic interactions between any two nitronyl nitroxide radicals: short NO...ON contacts usually lead to antiferromagnetic interactions, and NO...phenyl contacts to ferromagnetic ones. However, recent studies^[7] have shown that there is no correlation between the presence or absence of a dominant ferromagnetic interaction and the geometry of the NO...ON and/or C(sp²)-H...ON intermolecular short contacts, and that short NO...ON contacts are not always an indication of dominant antiferromagnetic interactions. One could also think about using qualitative procedures based on the so-called McConnell-I proposal,^[8] but previous studies have also found that this lacks a rigorous general foundation,^[9] and fails to describe the nature of the magnetic interactions in dimers of small radicals.^[10] Thus, it seems appropriate to carry out a systematic study of the magnetic interactions on the *p*-(MeS)PhNN crystal by using our recently proposed first principles, bottom-up procedure,^[11] aimed at rationalizing its bulk ferromagnetic properties in terms of reliable, computed microscopic interactions.

The mechanism of the magnetic interactions in a molecular crystal is fully rationalized once its *magnetic topology* has been determined.^[12] This requires the definition of: 1) the strength of the microscopic magnetic interactions between all unique pairs of radicals (the so-called J_{AB} parameters) and 2) the topological connectivity within the crystal of the non-negligible J_{AB} magnetic interactions. Once the magnetic topology has been determined, it is possible to identify the pathways that allow the propagation of the magnetic interactions over the whole solid.

Three different strategies have been used so far to obtain the value of the J_{AB} microscopic parameters in magnetic crystals: 1) a least-square fitting of the experimental data to a proposed model Hamiltonian,^[13] 2) a theoretical calcula-

Abstract in Catalan: *El mecanisme de les interaccions magnètiques en el cristall ferromagnètic (bulk) para-(metiltio)fenil nitronil nitròxid (YUJNEW) ha estat reinvestigat des d'un punt de vista teòric, usant únicament dades obtingudes a partir de càlculs ab initio i evitant qualsevol suposició a priori. Primer s'avaluen les possibles interaccions magnètiques microscòpiques (constants d'acoblament J_{AB}) d'entre tots els diferents parells de radicals existents en el cristall, i aleshores es calculen numèricament les propietats magnètiques macroscòpiques partint dels nivells d'energia de l'Hamiltonià de Heisenberg corresponent. Així doncs, connectem teoria i experiment mitjançant una aproximació bottom-up (d'informació microscòpica a macroscòpica) basada en primers principis. Aquesta estratègia de treball s'ha utilitzat per estudiar el magnetisme del YUJNEW usant estructures cristallines prèviament publicades a 298 i 114 K, i també una estructura determinada a 10 K per difracció de neutrons (documentada en aquest article). La topologia magnètica a 298 K és bidimensional, formada per plans que no interaccionen entre ells: en cada capa hi ha tres interaccions J_{AB} diferents (+0.24, +0.09 i -0.11 cm⁻¹) i entre capes una de numèricament negligible (+0.02 cm⁻¹). En canvi, la topologia magnètica a 114 i 10 K és tridimensional, amb dos constants J_{AB} intra-capça (+0.11 i +0.07 cm⁻¹ a 114 K; +0.22 i +0.07 cm⁻¹ a 10 K) i una entre capes (+0.07 cm⁻¹ a 114 K; +0.08 cm⁻¹ a 10 K) no negligibles. Tot i que aquesta topologia magnètica tridimensional és consistent amb el fet que el YUJNEW és un imant (bulk ferromagnet), a 114 K només s'obté una concordança qualitativa entre els valors calculats i les dades experimentals de la susceptibilitat magnètica $\chi T(T)$. La corba experimental $\chi T(T)$ únicament es pot reproduir amb les dades obtingudes a 10 K. Els resultats numèrics de la capacitat calorífica presenten un màxim entorn 0.12 K; valor molt proper a la temperatura crítica del YUJNEW estimada experimentalment de 0.20 K.*

tion using ab initio methods, and 3) a combination of 1) and 2), in which calculated parameters are used as a starting point to fit experimental data. Our first principles, bottom-up analysis clearly belongs to the second group of strategies. It begins by systematically computing all unique non-negligible J_{AB} pair interactions.^[14] The magnetic topology is then obtained by connecting the radicals having non-negligible J_{AB} parameters. Macroscopic magnetic properties of the solid (e.g., magnetic susceptibility or heat capacity) are computed from the eigenvalues of a Heisenberg Hamiltonian, which quantitatively represents the topology of the magnetically non-negligible J_{AB} interactions within the crystal. We believe that this micro-to-macro or bottom-up strategy will become a practical tool for the rational design of molecular magnets, once our knowledge of the microscopic molecular interactions and control of crystal packing improve.

In summary: in this work, we re-investigate the nature of the magnetic interactions in the *p*-(MeS)PhNN crystal from first principles. We study the 298, 114 and 10 K crystal structures to evaluate whether (and if so, how) temperature affects the computed properties of organic molecular magnets. To our knowledge, such *quantitative* evaluation of the changes induced by temperature on the mechanism of the magnetic interaction of a given crystal has not been reported up to now. Our results show that while the topology at 298 K is two-dimensional (2D), the low-temperature structures (114 and 10 K) are three-dimensional (3D), which agrees with the experimental behavior. The trends in thermal expansion of the *p*-(MeS)PhNN crystal suggest that magnetic topology in the vicinity of the transition temperature (0.20 K) will be the same as at 10 K. We will also show that the computed magnetic susceptibility and heat capacity obtained using our procedure fully reproduce the experimental values of these macroscopic magnetic properties.

Computational Methods

Since we have described our first principles, bottom-up methodology in detail before,^[11a] we will only summarize the main steps in physical terms here.

The basic idea is to determine the magnetic topology of a crystal from the values of microscopic J_{AB} pair interactions between its constituent radicals, and then to compute macroscopic magnetic properties from the energy levels of the corresponding Heisenberg Hamiltonian [Eq. (1)], in which \hat{S}_A is the spin operator associated with the radical *A*, and \hat{I}_{AB} is the identity operator.

$$\hat{H} = - \sum_{A,B}^N J_{AB} (2\hat{S}_A \cdot \hat{S}_B + \frac{1}{2}\hat{I}_{AB}) \quad (1)$$

Practically, our approach involves the following consecutive steps:

- 1) A detailed analysis of the crystal packing to identify, in an unbiased and systematic way, all unique relevant AB pairs of radicals. We deliberately select more pairs than the first nearest neighbors, which are the usual candidates in the literature.
- 2) The ab initio computation of the J_{AB} magnetic interactions for all pairs of radicals selected in the previous step.
- 3) Determination of the magnetic topology of the crystal, by inspection of the connectivity of the non-negligible J_{AB} values for each radical pair. Each radical molecule can be seen as a radical site, connected to another when $|J_{AB}|$ is larger than a given threshold (estimated as

$|0.05| \text{ cm}^{-1}$ in our calculations). Then, one searches for the (finite-sized) minimal magnetic model space that describes the magnetic interactions of the whole crystal in a balanced way. The radical centers of the minimal magnetic model space define a spin space, which is used to compute the matrix representation of the Heisenberg Hamiltonian [Eq. (1)]. The J_{AB} parameters required in that matrix representation are those computed in step 2.

- 4) As a final step, the Heisenberg Hamiltonian matrix is fully diagonalized and the whole set of eigenvalues is obtained. That set of eigenvalues (the energy spectrum) is used to compute the magnetic susceptibility $\chi(T)$ and/or heat capacity $C_p(T)$ using standard statistical mechanics.

The minimal magnetic model space must be small enough to keep the size of the Heisenberg Hamiltonian matrix manageable (currently $N=16$ spin sites), but it must also contain all of the important magnetic pathways detected within the crystal. To test the validity of our minimal magnetic model space, we checked the convergence of our results (e.g., χ vs T) by replicating the model space along all three crystallographic directions: if the minimal magnetic model space is properly chosen, the computed $\chi(T)$ values from such extended models should rapidly converge to the computed $\chi(T)$ values from the minimal model, which in turn should approach the experimental $\chi(T)$ data. From our experience, the most essential issue in our procedure is the selection of a proper subset of J_{AB} pair interactions within the crystal capable of describing its magnetic topology evenly.

As already mentioned, constructing the matrix of the Heisenberg operator requires the values of the microscopic J_{AB} pair interactions. These are computed, by using ab initio methods, from the energy difference between the high and low spin states of the pair of radicals. In the case of the *p*-(MeS)PhNN, a doublet radical, the value of J_{AB} for any pair is obtained by subtracting the energy of the most stable open-shell singlet (E_{BS}^S) and triplet (E^T) states at the pair geometry, using the broken-symmetry approximation^[15] to compute the energy of the open-shell singlet state [Eq. (2)].

$$J_{AB} = E_{BS}^S - E^T \quad (2)$$

This expression is obtained by equating the expression of the singlet–triplet energy difference obtained from the original formulation of the broken-symmetry approximation developed for the UHF method [Eq. (3)] and the expression of the singlet–triplet energy difference [Eq. (4)] computed using the Heisenberg Hamiltonian [Eq. (1)].

$$\Delta E^{S-T} = 2(E_{BS}^S - E^T)/(1 + S_{ab}^2) \quad (3)$$

$$\Delta E^{S-T} = 2J_{AB} \quad (4)$$

The J_{AB} term in Equation (2) results from the fact that in through-space magnetic interactions the SOMO orbital of one radical of the dimer presents a very small overlap ($S_{ab} \approx 0$) with the SOMO of the other radical. The E_{BS}^S and E^T energy values were computed by using the UB3LYP functional^[16] and the 6-31+G(d) basis set^[17] (a 10^{-8} convergence criterion on the total energy and 10^{-10} on the integrals was used to ensure enough accuracy in the computation of the J_{AB} parameters). Note that our expression is equivalent to the use of $J_{AB} = 2(E_{BS}^S - E^T)$ commonly employed with the $\hat{H} = -\sum_{A,B} J_{AB} \hat{S}_A \cdot \hat{S}_B$ Heisenberg Hamiltonian.^[15] In the case of strong overlap between the two magnetic orbitals, as in most through-bond magnetic interactions, overlap should be taken into consideration in Equation (3), and the energy difference should be divided by two.^[15] It has also been found that when the broken-symmetry approach is applied in the context of transition-metal complexes and DFT methodology, better agreement against the experimental J_{AB} values is obtained when $\Delta E^{S-T} = E_{BS}^S - E^T$. This has been attributed by some to error compensation and by others to some intrinsic behavior of the DFT functionals.^[18] All DFT calculations performed in this study were carried out using the Gaussian-98 package.^[19]

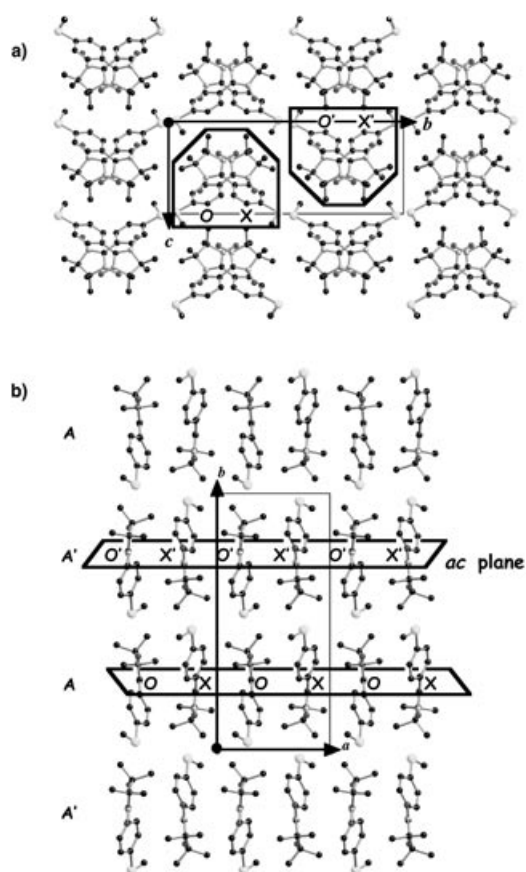


Figure 1. a) View of the crystal packing for YUJNEW along the a crystallographic direction (hydrogen atoms are not shown). Within the unit cell, four p -(MeS)PhNN radicals are arranged in two pairs O–X and O'–X' (encircled). b) Snapshot of the main packing motif of YUJNEW crystal: ac planes stacked along the b axis in an AA'AA' sequence.

Results and Discussion

Crystal packing analysis of the p -(MeS)PhNN crystal: The crystal structure of the p -(MeS)PhNN radical has been fully reported at 298^[2] and 114 K^[5] (refcodes YUJNEW10 and YUJNEW11 in the CCSD database, respectively^[20]). Besides these two crystal structures, cell parameters were also reported for the crystal at 10 K, although without fractional coordinates. In this work we report these fractional coordinates (we will identify this crystal as YUJNEW10K).

The 298, 114, and 10 K structures present the same crystal symmetry ($P2_1/a$) and relative disposition of radicals within the crystal structure, which is shown in Figure 1. However, the thermal compression of the unit cell is slightly anisotropic (see Table 1): the b axis shrinks by 0.345 Å on going from 298 to 114 K, and by 0.089 Å in the 114 to 10 K transition; the a axis decreases by 0.097 and 0.104 Å for the same transitions, while the c axis increases by 0.118 Å and afterwards shrinks by 0.031 Å. An analysis of the packing shows that there are four p -(MeS)PhNN radicals per unit cell ($Z=4$) arranged in two pairs (see Figure 1a for encircled pairs O–X and O'–X'). The radical molecules in each of these pairs are in an up–down orientation. The two radicals are connected by intermolecular C–H $\cdots\pi$ bonds, involving the phenyl

Table 1. Cell parameters reported at 298 K, 114 K, and 10 K for p -(MeS)PhNN crystal.

T [K]	a [Å]	b [Å]	c [Å]	β [°]	Ref.
295	9.437	19.827	8.516	113.66	[2]
114	9.340	19.482	8.634	115.13	[5]
10	9.236	19.393	8.603	114.94	[4]

group of one radical and the ONCNO group of the five-membered NN ring of the other. The main packing motif of this crystal is the formation of planes along the ac axes, stacked along the b axis in an AA'AA' sequence (Figure 1b) in such a way that the X–X' and O–O' radicals form chains linked by C–H \cdots S bonds (involving methyl and thiomethyl groups). Though only partially observed in the bc projection (Figure 1a), neighboring radicals (O–X and O'–X') are oriented nearly perpendicular to each other within each ac plane. In this packing, the NN ring of the O radicals sits on top of the phenyl ring of the X radicals, with one of the NO oxygen atoms of one radical nearly on top of the NN ring C(sp²) atom of the other radical, at an ONCNO \cdots C(sp²) distance of 4.208 Å (J^i , J^{ii} , in Figure 2a and 2b, with O–X radical molecules related by a glide plane). Along the c axis the X and O radicals are held by simultaneous C(sp²)–H \cdots ON and C(sp³)–H \cdots ON bonds (from the C atoms of the phenyl ring and the thiomethyl groups to the NO groups, J^{iii} in Figure 2a and 2b). The change with temperature of the shortest contact distances (Tables 2–4) and angles is non-uniform, due to the already mentioned anisotropic change of the cell parameters

Previous empirical magnetic models of the p -(MeS)PhNN crystal:

Based on the empirical observation that short NO \cdots ON contacts usually lead to antiferromagnetic interactions, and short NO \cdots phenyl contacts to ferromagnetic interactions, the original authors of reference [2] proposed the two-dimensional magnetic model shown in Figure 2a. This model involves three ferromagnetic J^i , J^{ii} , and J^{iii} parameters, as they are associated to radical pairs oriented so that the shortest contacts are of the NO \cdots phenyl type (Figure 2b). Initially, no magnetic interaction was proposed between the ac planes (i.e., along the b axis) based only on geometrical considerations (the ONCNO groups are more than 6 Å apart). However, on the basis of EPR data, the same authors revised their initial magnetic model and concluded that an interplane interaction should exist.^[2] Subsequently,^[3] the same authors proposed a three-dimensional magnetic model (Figure 2c) of weakly interacting square planes, in which the interaction within the planes was J and that between the planes was J' . The in-plane J parameters of this 3D model should be taken as an effective J that averages the three ferromagnetic J^i , J^{ii} , and J^{iii} parameters of the 2D model (by doing this averaging, the J parameters lose their direct connection with the microscopic J_{AB} radical-pair parameters described in the Computational Methods).

Besides proposing a feasible magnetic model, the authors of references [2,3] fitted the available experimental $\chi(T)$ data to 1) the Curie–Weiss law ($\theta = +0.32$ K^[21]) and 2) a numerical series expansion for the spin $1/2$ Heisenberg model

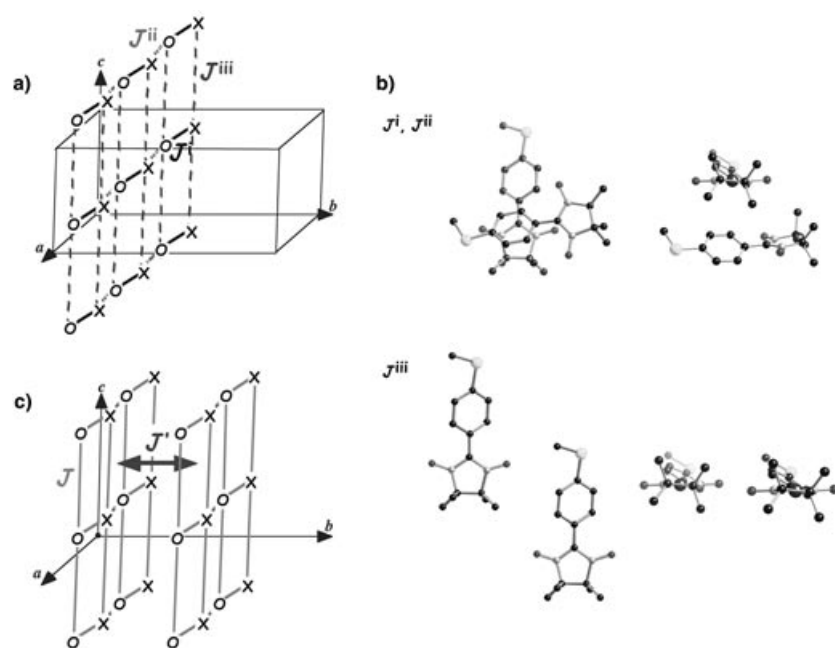


Figure 2. a) Initial magnetic topology (2D *ac* layer) of YUJNEW proposed by the original authors,^[2] in which each *p*-(SMe)PhNN radical molecule is replaced by a point site for simplicity (J , J^{ii} , and J^{iii} magnetic interactions are shown). b) Geometry of the pair of radicals involved in the suggested J^i , J^{ii} , J^{iii} interactions (note that $J^i = J^{ii}$ by symmetry). c) Final magnetic topology (3D) suggested by the original authors^[3] in order to interpret the available experimental data (J , J' magnetic interactions are shown).

Table 2. Shortest intermolecular distances for radical pairs d1–d9 for the 298 K structure of YUJNEW (atoms labelled according to Scheme 1). Radical pairs d1–d5 were selected on the basis of ONCNO...ONCNO distance (in bold) (although d1, d3 and d4 could have been chosen according to the shortest NO...SMe distance (in italics), all remaining NO...ON distances were shorter in average). Radical pairs d6 and d7 were selected on the basis of the ONCNO...SMe distance (in bold), and d8 and d9 on the basis of the MeS...SMe distance (in bold). UB3LYP-BS/6–31+G(d) values for $J_{AB}(d_i)$ are also given.

	$d(\text{NO}\cdots\text{ON})$ [Å]	$d(\text{C}_1\cdots\text{C}_1)$ [Å]	$d(\text{NO}\cdots\text{S}_1\text{Me})$ [Å]	$d(\text{MeS}_1\cdots\text{S}_1\text{Me})$ [Å]	$J(d_i)$ [cm ⁻¹]
d1	4.71 , 4.94, 6.56, 7.18	4.81	<i>4.60</i> , 6.37, 7.40, 10.18	9.83	+0.24
d2	5.69 , 8.04, 9.13, 11.04	7.96	6.71, 6.97, 9.86, 13.80	11.70	+0.09
d3	5.87 , 8.52(2), 12.38	8.52	<i>4.63</i> , 9.20, 12.50, 14.56	8.52	-0.11
d4	6.96 , 10.43, 10.67, 12.97	9.99	<i>6.85</i> , 6.87, 13.74, 17.57	12.81	$\cong 10^{-2} $
d5	7.02 , 10.98(2), 15.35	11.17	12.56(2), 15.94(2)	19.03	$\cong 10^{-2} $
d6	10.68, 10.96, 15.29(2)	12.53	4.20 , 8.76, 14.78, 16.71	9.93	+0.02
d7	11.17, 12.66(2), 15.45	12.08	6.99 (2), 10.11(2)	7.85	$\cong 10^{-2} $
d8	13.27, 13.48(2), 15.17	12.76	7.34(2), 8.78(2)	4.48	$\cong 10^{-2} $
d9	16.07(2), 16.65, 16.79	15.35	10.24(2), 10.53(2)	5.32	$\cong 10^{-2} $

Table 3. Shortest intermolecular distances for radical pairs d1–d9 for the 114 K structure of YUNEW (atoms labelled according to Scheme 1). Radical pairs d1–d5 were selected on the basis of ONCNO...ONCNO distance (in bold) (although d1, d3 and d4 could have been chosen according to the shortest NO...SMe distance (in italics), all remaining NO...ON distances were shorter in average). Radical pairs d6 and d7 were selected on the basis of the ONCNO...SMe distance (in bold), and d8 and d9 on the basis of the MeS...SMe distance (in bold). UB3LYP-BS/6–31+G(d) values for $J_{AB}(d_i)$ are also given.

	$d(\text{NO}\cdots\text{ON})$ [Å]	$d(\text{C}_1\cdots\text{C}_1)$ [Å]	$d(\text{NO}\cdots\text{S}_1\text{Me})$ [Å]	$d(\text{MeS}_1\cdots\text{S}_1\text{Me})$ [Å]	$J(d_i)$ [cm ⁻¹]
d1	4.77 , 4.82, 6.74, 7.23	4.83	4.29, 6.35, 7.1, 10.10	9.64	+0.11
d2	5.65 , 7.97, 9.26, 11.12	7.97	6.72, 6.80, 9.70, 13.67	11.55	+0.07
d3	5.95 , 8.63(2), 12.52	8.63	4.76, 9.36, 12.59, 14.66	8.63	-0.02
d4	6.79 , 10.22, 10.59, 12.81	9.85	6.69, 6.89, 13.62, 17.51	12.73	$\cong 10^{-2} $
d5	6.52 , 10.53(2), 14.91	10.70	12.15(2), 15.55(2)	18.71	$\cong 10^{-2} $
d6	10.52, 10.78, 15.12, 15.15	12.35	4.00 , 8.59, 14.65, 16.58	9.75	+0.07
d7	11.13, 12.71(2), 15.57	12.14	6.87 (2), 10.11(2)	7.68	$\cong 10^{-2} $
d8	13.24, 13.49(2), 15.22	12.72	7.35(2), 8.83(2)	4.61	$\cong 10^{-2} $
d9	16.14(2), 16.75, 16.84	15.40	10.24(2), 10.51(2)	5.12	$\cong 10^{-2} $

on the square lattice with a mean field correction for inter-lattice interactions ($J = +0.18$ K, $J' \approx +0.042$ K^[6]).

Evaluation of the magnetic topology of the *p*-(MeS)PhNN crystal at 298 K (YUJNEW10): We began our quantitative study of the magnetism of YUJNEW10 by selecting all possible radical pairs that could give rise to a non-negligible magnetic interaction (Step 1). Polarized neutron diffraction and X-ray/neutron studies^[4,5] have shown that most of the spin density (87.7%) of this radical is located on the ONCNO group of the five-membered NN ring, with a very small amount on the C atoms of the NN group itself, the phenyl ring and the thiomethyl group (the S atom of the thiomethyl group is however found to have a negligible spin population). The same spin distribution is obtained by B3LYP calculations, in good agreement with the general trends found in the nitronyl nitroxide NN radicals.^[22]

Given the spin distribution, we selected for our study all radical pairs in which the ONCNO...ONCNO contacts have distances below 7.4 Å. Furthermore, as there are suggestions that the MeS atoms could play some role in the magnetism of this crystal, we also selected all radical pairs whose ONCNO...SMe and MeS...SMe contacts are below 6.9 and 9.0 Å, respectively (notice that the same radical pairs are selected if using ONCNO...MeS and SMe...MeS distances as a cutoff criteria). Such a long-range cutoff for the contacts included all first nearest neighbors and the closest second-nearest neighbors. Nine radical pairs were selected in this way (Figures 3a,b and 4), identified as d1–d9. There are two groups of pairs: d1–d3, in which the two radicals are lo-

Table 4. Shortest intermolecular distances for radical pairs d1–d3 and d6 for the 10 K structure of YUNEW (atoms labelled according to Scheme 1). UB3LYP-BS/6-31+G(d) values for $J_{AB}(di)$ are also given.

	$d(\text{NO}\cdots\text{ON})$ [Å]	$d(\text{C}_1\cdots\text{C}_1)$ [Å]	$d(\text{NO}\cdots\text{S}_1\text{Me})$ [Å]	$d(\text{MeS}_1\cdots\text{S}_1\text{Me})$ [Å]	$J(di)$ [cm ⁻¹]
d1	4.76 (2), 6.74, 7.17	4.79	4.24, 6.27, 7.06, 10.00	9.58	+0.22
d2	5.64 , 7.95, 9.27, 11.10	7.96	6.74, 6.69, 9.67, 13.62	11.50	+0.07
d3	5.95 , 8.60(2), 12.47	8.60	4.76, 9.35, 12.55, 14.59	8.60	-0.02
d6	10.44, 10.72, 15.06(2)	12.27	3.95 , 8.54, 14.59, 16.54	9.71	+0.08

cated in the *ac* plane, and d4–d9, in which the two radicals are placed in consecutive *ac* planes. The view in Figure 3 is similar to that chosen in Figure 2 to allow an easy comparison between them. The values of the key intermolecular distances for each pair are collected in Table 2.

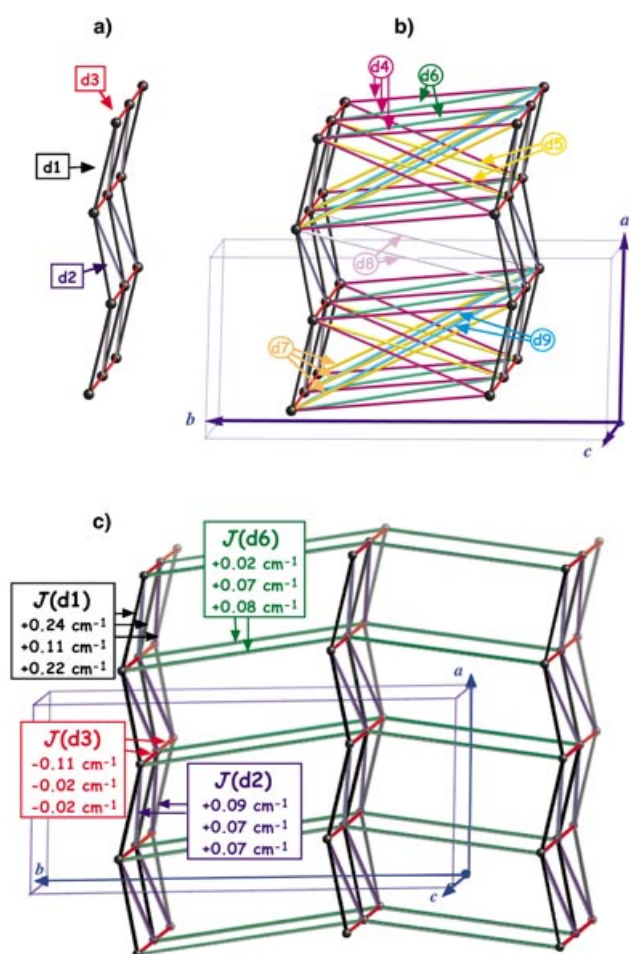


Figure 3. a,b) Schematic view of YUNEW crystal in terms of potential d1–d9 magnetic pair interactions selected for computation of $J(di)$ values (*p*-(MeS)PhNN radicals replaced by point sites). All potential magnetic pair interactions d_i are drawn as a line. These lines are pictured in different colors to distinguish among different pairs of radicals: a) within an *ac* layer ($i=1-3$) and b) between any two *ac* layers ($i=4-9$). c) Magnetic topology for YUNEW defined by four non-negligible $J(di)$ dimeric interactions ($i=1-3, 6$). The computed values of $J(di)$ magnetic pair interactions are given at 298 K (upper value), 114 K (middle value), and 10 K (lower value). At 298 K, the magnetic topology of YUNEW consists of non-interacting two-dimensional *ac*-layers (+0.24, +0.09 and -0.11 cm⁻¹). At 114 K and 10 K, the magnetic topology of YUNEW is clearly three-dimensional (intra/inter *ac* planes: +0.11, +0.07/+0.07 and +0.22, +0.07/+0.08 cm⁻¹, respectively).

The computation of the value of the microscopic magnetic interaction J_{AB} for each radical pair d_i was done (Step 2) at the geometry of the pair found in the YUNEW10 crystal. These J_{AB} values are collected in the last column of Table 2. At this geometry, the three in-plane radical pairs d1–d3 are the main contributors to the magnetic interaction of YUNEW10, the first two ferromagnetically (+0.24 and +0.09 cm⁻¹) and the last one antiferromagnetically (-0.11 cm⁻¹). There is also a much smaller magnetic contribution from the interplane pairs (d6), whose sign and size (+0.02 cm⁻¹, Table 2) lies below the limit of accuracy expected for our computations, and which can thus be neglected.^[23] Therefore, the *p*-(MeS)PhNN crystal at 298 K has the 2D magnetic topology (Step 3) depicted in Figure 3c (upper $J(di)$ values), with a negligible interplane magnetic interaction. Therefore, it does not have the 3D character detected experimentally. In a first qualitative approach, one expects that these 2D planes should present a dominant ferromagnetic behavior in the magnetic susceptibility curve, because the ferromagnetic in-plane interactions are twice as strong as the antiferromagnetic in-plane interactions. However, a proper estimation of such a curve is only possible after a quantitative computation (Step 4, discussed below in the section on the computation of the macroscopic magnetic properties), which shows that the 298 K magnetic topology does not behave as a ferromagnet in the 0–3 K region.

We first comment on the main features of the sign and size of the non-negligible J_{AB} parameters. The sign of the $J(d1)$ pair (+0.24 cm⁻¹) is consistent with that predicted by the McConnell-I proposal. However, the antiferromagnetic character of $J(d3)$ violates the McConnell-I proposal: with a shortest NO \cdots ON distance of 5.87 Å it should be negligible. The presence of a magnetic interaction at such a large NO \cdots ON distance indicates that atoms other than the ONCNO group should play a role in the magnetic interaction, even if no significant amount of spin is located on them, in agreement with previous suggestions.^[7] It is also important to stress here that there is no direct correspondence between the J parameter obtained from the least-square fitting of the magnetic susceptibility curves ($J = +0.18$ K^[3]) and the microscopic in-plane $J(d1)$, $J(d2)$, and $J(d3)$ (compare Figures 2c and 3c). Therefore J should be taken as an effective parameter that represents an average of the $J(d1)$, $J(d2)$, and $J(d3)$ in-plane pair interactions (whose values are +0.24, +0.09, and -0.11 cm⁻¹, respectively). On the other hand, one can relate $J^i = J^{ii} = J(d1)$ and $J^{iii} = J(d3)$ (radical molecules related by glide-plane and *c*-translation, respectively, compare Figures 2a and 3c). Thus, the initial empirical model of the magnetic topology at 298 K was appropriate and only the $J(d2)$ pair interaction was missing. However, we will next see that $J(d1)$, $J(d2)$, and $J(d3)$ allow the shape of the experimental magnetic susceptibility curve to be reproduced only in the 3–280 K region, but not below that temperature range. Finally, there might be a direct connection between J^i (+0.042 K) and $J(d6)$ (+0.02 cm⁻¹), but

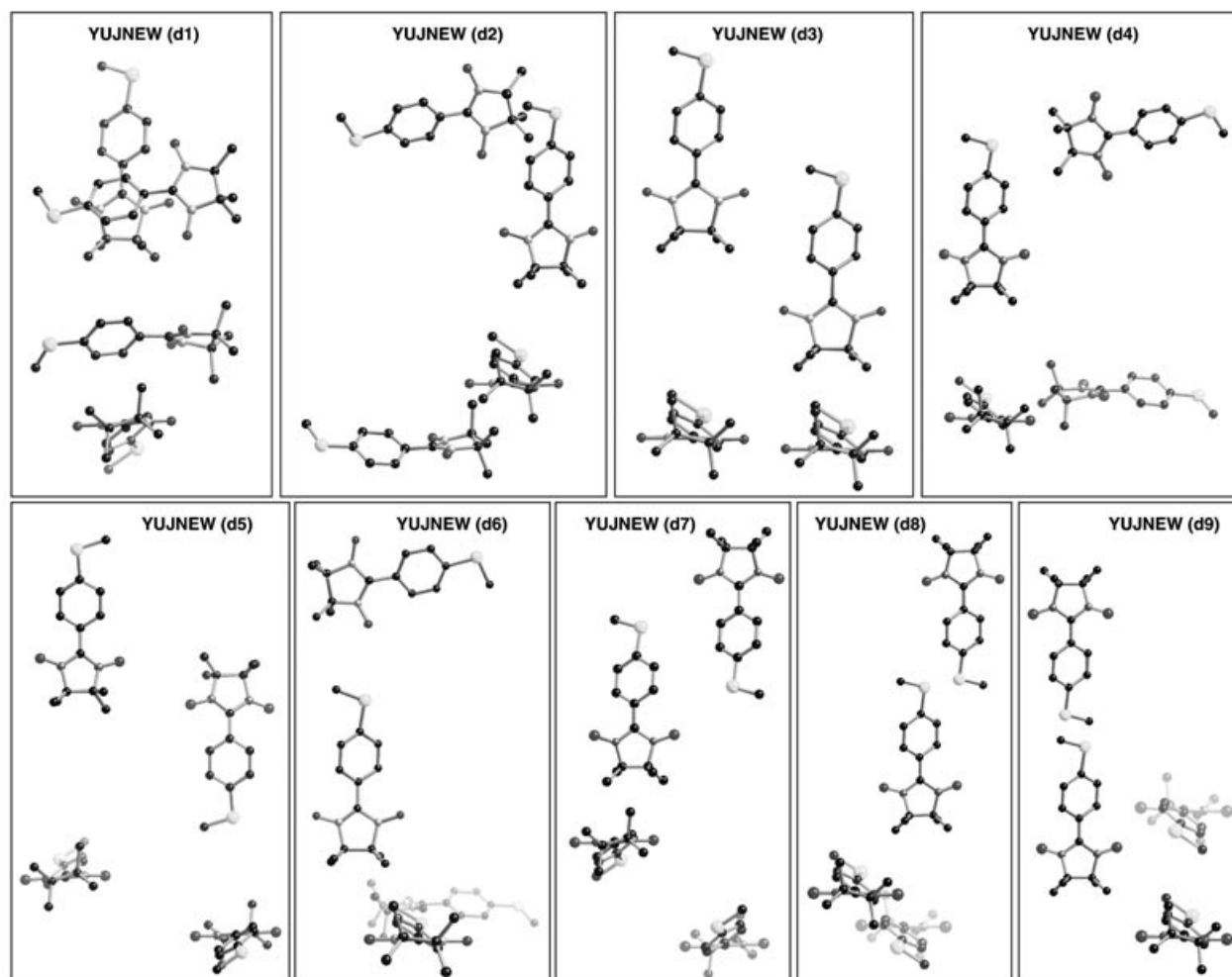


Figure 4. Geometrical arrangement of the nine dimeric interactions d_i selected as candidates to be magnetically important. For each d_i pair of radicals, the upper/lower figure shows the dimer with the NN-plane parallel/perpendicular to the plane of the figure.

the original authors did not associate J to any radical pair AB within the crystal.^[3] Notice also that in YUJNEW10 the interplane magnetic interactions are numerically too small.

Summarizing, the 298 K structure of the *p*-(MeS)PhNN crystal might give rise to 2D ferromagnetism, a fact that is not consistent with the 3D bulk ferromagnetism detected experimentally in *p*-(MeS)PhNN crystals below 0.20 K. However, as we will show in the next section, the small changes in the crystal packing when lowering the temperature are enough to generate a change in the magnetic topology of the crystal, which will then become a 3D ferromagnet.

Evaluation of the magnetic topology of the *p*-(MeS)PhNN crystal at 114 K and 10 K: We have also evaluated the magnetic topology of the *p*-(MeS)PhNN crystal determined at 114 K (YUJNEW11). As mentioned before, the 298 and 114 K crystal packing are similar, and the relative orientation of the molecules is preserved. Therefore, it is not surprising that the radical pairs obtained in Step 1 when applying our procedure to the 114 K crystal structure give a one-to-one correspondence to the d1–d9 pairs obtained for the 298 K structure (the changes in the intermolecular distances

can be analyzed by comparing Tables 2 and 3). Given the $J(d_i)$ values at 114 K, we focused on the d1, d2, d3 and d6 pairs. Although the changes in the geometry of these pairs are small (Tables 2 and 3) they induce significant modifications in the associated $J(d1)$, $J(d2)$, $J(d3)$, and $J(d6)$ parameters (Table 3) and in the magnetic topology. Comparing the results at 114 K to those at 298 K one realizes that 1) $J(d1)$ has decreased and becomes similar in strength to $J(d2)$ and $J(d6)$; 2) $J(d2)$ decreases slightly; 3) $J(d3)$, the only antiferromagnetic pair interaction at 298 K, becomes numerically negligible at 114 K; and 4) $J(d6)$ has been strengthened more than threefold.

The increase in the strength of $J(d6)$ ($+0.02 \text{ cm}^{-1} \rightarrow +0.07 \text{ cm}^{-1}$) can be anticipated from the sharp decrease in the size of the b cell parameter. Similarly, one would try to justify the decrease in the ferromagnetic value of $J(d1)$ ($+0.24 \text{ cm}^{-1} \rightarrow +0.11 \text{ cm}^{-1}$) and $J(d2)$ ($+0.09 \text{ cm}^{-1} \rightarrow +0.07 \text{ cm}^{-1}$) in terms of $\text{NO}\cdots\text{C}(\text{sp}^2)$ and $\text{NO}\cdots\text{ON}$ distances. However, this is not possible, as for example, for the d1 pair, the $\text{NO}\cdots\text{C}(\text{sp}^2)$ distance of 4.251 Å at 298 K becomes 4.208 Å at 114 K; one would therefore expect an increase of the $J(d1)$ value, but it decreases instead. This illustrates the difficulties in predicting changes in the $J(d_i)$ values by using

simple geometrical considerations and McConnell-I or monoparametric magneto-structural correlations.

The magnetic topology of the *p*-(MeS)PhNN crystal at 114 K (YUJNEW11) resulting from the $J(d_i)$ computations is depicted in Figure 3c (middle $J(d_i)$ values). It is clearly 3D, with two in-plane ferromagnetic interactions (of values $+0.11$ and $+0.07$ cm⁻¹) and one interplane ferromagnetic interaction ($+0.07$ cm⁻¹). No sizable antiferromagnetic interaction is present, as $J(d_3)$ lies now below the accuracy limit and can thus be neglected. This magnetic topology represents a remarkable change from that discussed above for the 298 K crystal. As we will next discuss, the magnetic susceptibility curve predicted using the 114 K or 298 K magnetic topologies differs below 3 K, and only the 114 K magnetic topology reproduces the experimental magnetic susceptibility curve across the whole range of temperatures.

Cell parameters have been previously reported for a 10 K crystal, closer to the critical temperature (0.20 K) than 298 and 114 K. We have obtained the fractional coordinates for this 10 K crystal, which are reported in Table 5. This allowed us to carry out the same quantitative analysis on the 10 K crystal as described above for the 298 and 114 K crystals.

Table 5. Fractional coordinates of *p*-(MeS)PhNN crystal at 10 K. Crystal symmetry ($P2_1/a$) and cell parameters given in Table 1.

Atom	<i>x</i>	<i>y</i>	<i>z</i>	U_{eq}
S1	2560(10)	336(2)	9772(4)	0.47
N1	2899(4)	3499(1)	6213(1)	1.08
N2	3016(3)	2761(1)	4324(1)	0.83
O1	2953(5)	3764(1)	7586(2)	1.47
O2	3062(6)	2198(1)	3577(2)	1.21
C1	3041(5)	2826(1)	5906(2)	0.97
C2	3094(4)	2252(1)	7008(2)	0.37
C3	2289(5)	2306(1)	8058(2)	0.63
C4	2117(5)	1735(1)	8944(3)	1.56
C5	2765(5)	1101(1)	8816(2)	0.93
C6	3662(5)	1057(1)	7859(2)	0.50
C7	3812(5)	1619(1)	6944(3)	1.06
C8	2464(5)	3927(1)	4616(2)	0.95
C9	3010(7)	3446(1)	3519(2)	0.37
C10	638(5)	4022(1)	3867(3)	0.71
C11	4721(6)	3583(1)	3788(2)	0.88
C12	3312(6)	4620(1)	5077(3)	1.42
C13	1898(7)	3418(1)	1619(3)	0.58
C14	-3533(5)	4391(1)	975(3)	0.80
H1	1757(10)	2792(2)	8161(4)	2.92
H2	1486(10)	1788(2)	9712(5)	3.27
H3	4240(9)	576(2)	7819(4)	2.19
H4	4437(13)	1575(3)	6153(6)	3.37
H5	231(9)	4341(3)	2713(4)	2.04
H6	362(10)	4292(2)	4816(5)	3.44
H7	32(10)	3533(2)	3548(4)	2.91
H8	4775(10)	4061(2)	3146(5)	3.44
H9	5114(10)	3163(3)	3215(5)	3.41
H10	5571(9)	3616(2)	5136(5)	2.11
H11	3193(10)	4882(3)	3902(5)	3.20
H12	4525(12)	4577(3)	5944(7)	2.73
H13	2742(11)	4949(3)	5664(6)	3.25
H14	1786(10)	3931(2)	1065(4)	3.18
H15	758(16)	3238(3)	1379(6)	3.82
H16	2358(14)	3071(3)	983(5)	3.96
H17	-2874(10)	4020(2)	1966(5)	2.82
H18	-4654(10)	4170(3)	133(5)	2.87
H19	-3698(9)	4861(2)	1579(4)	2.81

An analysis of the packing of the 114 K and 10 K structures reveals their similarity: there are small changes in the cell parameters, and little difference between the intermolecular distances reported in Tables 3 and 4. It is thus not surprising that the pairs selected in Step 1 of our procedure are the same in the 114 K and 10 K structures. Given such similarity, we only computed the values of the microscopic J_{AB} parameters for the four pairs found relevant for the magnetism of *p*-(MeS)PhNN crystal at 114 K (and also at 298 K). The values of these $J(d_i)$ parameters for the 10 K structure are collected in the last row of Table 4. These values present almost no change for $J(d_2)$, $J(d_3)$, and $J(d_6)$ ($+0.07$, -0.02 , and $+0.08$ cm⁻¹, respectively), but double that found in the 114 K structure for the d1 pair ($+0.22$ cm⁻¹). This fact supports the relevance of using low-temperature crystal structures in the analysis of the magnetism in purely organic crystals. However, it does not modify the magnetic topology at 10 K relative to the 114 K structure, which again shows a clear 3D character (Figure 3c, lower $J(d_i)$ values). As we do not expect large changes in the crystal cell parameters when lowering the temperature from 10 to 0.20 K, we are confident that Figure 3c (lower $J(d_i)$ values) depicts the magnetic topology of the YUJNEW crystal in the range of temperatures in which it presents bulk ferromagnetic properties.

Computation of the macroscopic magnetic properties of *p*-(MeS)PhNN crystal—connecting microscopic computed information to macroscopic measurements: To study the macroscopic magnetic properties (Step 4) of the *p*-(MeS)PhNN crystal at any temperature, we first have to select a physically appropriate minimal magnetic model.

At 298 K (YUJNEW10, Figure 3c upper $J(d_i)$ values), the magnetic topology consists of non-interacting 2D *ac* layers ($+0.24$, $+0.09$, and -0.11 cm⁻¹). Thus, we will first focus on reproducing the magnetic topology along the *ac* planes. As shown in Figure 5a, an evident choice for the magnetic building block is a four-site unit, which we will call $(1a,1c)$. This minimal magnetic model is capable of generating the YUJNEW10 (*na,mc*) magnetic topology by replicating itself *n* times along the *a* axis and *m* times along the *c* axis. If our minimal model is correct, as one propagates it by translation along the *a* and *c* axes the computed $\chi(T)$ values should converge towards a limit, close to the experimental $\chi(T)$ result. We found such convergence (see Supporting Information Figure S1), using the $(2a,1c)$, $(3a,1c)$, and $(4a,1c)$ models to test the convergence along the *a* axis, the $(1a,2c)$, $(1a,3c)$, and $(1a,4c)$ models to test the *c* axis convergence, and the $(3a,3c)$ model to check the simultaneous convergence along the two axes (see Figure 5a for models).

For the 114 K and 10 K crystals (YUJNEW11 and YUJNEW10 K, Figure 3c: middle and lower $J(d_i)$ values, respectively), the natural model that simultaneously describes the in- and interplane magnetic interactions might appear to be model $(1a,1c)_2$, a parallelogram in which two $(1a,1c)$ models are connected by $J(d_6)$ interactions (Figure 5b). However, as the $J(d_3)$ parameter at 114 K and 10 K is numerically negligible, an alternative model, $(1a,1c)_2'$ (Figure 5b) was proposed. Convergence was checked by extending $(1a,1c)_2$

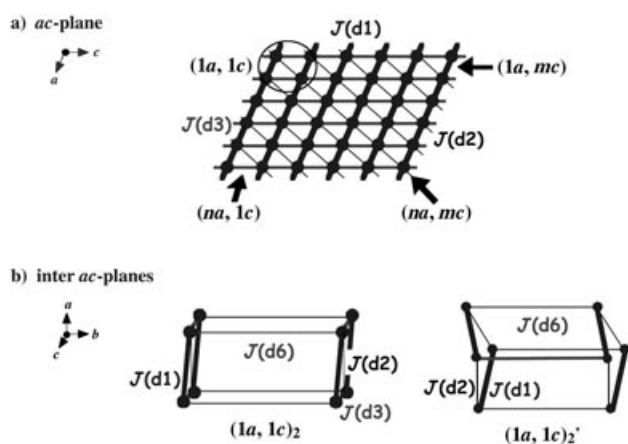


Figure 5. Models used to study the magnetism of YUJNEW at a) 298 K (non-interacting ac layers), and b) 114 K and 10 K (3D magnetic topology). In a), $(1a,1c)$ is the smallest model required to describe the magnetic topology of the ac -plane. Models $(2a,1c)$, $(3a,1c)$... $(na,1c)$ are the extension of such minimal magnetic $(1a,1c)$ model along the a axis; $(1a,2c)$, $(1a,3c)$... $(1a,mc)$ along the c axis; and $(2a,2c)$, $(3a,3c)$... (na,mc) along the a and c axes simultaneously. In b), the three-dimensionality of the magnetic topology at 114 K and 10 K is described by introducing two minimal eight-site magnetic models: $(1a,1c)_2$ and $(1a,1c)_2'$. Note that minimal magnetic $(1a,1c)$ and $(1a,1c)_2/(1a,1c)_2'$ models are capable of generating YUJNEW 2D and 3D magnetic topologies at 298 K and 114 K/10 K, respectively, by replicating themselves.

and $(1a,1c)_2'$ along the a , b , and c crystallographic axes (Supporting Information, Figure S2 and S3).

We computed the matrix representation of the Heisenberg spin Hamiltonian for each minimal magnetic model. The resulting energy levels were used to obtain the macroscopic susceptibility $\chi(T)$ (0.05–280 K) and heat capacity $C_p(T)$ (0.05–3.5 K) (Figures 6 and 7, respectively). Notice that, for clarity, Figures 6 and 7 only show data within the 3–100 K/0.05–3.0 K range for $\chi T(T)$, and within the 0.05–1.4 K range for $C_p(T)$.

Several observations can be made concerning the magnetic susceptibility data:

- 1) The shape of the $\chi T(T)$ curve computed using the 298 K $J(di)$ parameters (model $(1a,1c)$ in Figure 6) does not behave as a dominant ferromagnet below 1 K, due to the presence of antiferromagnetic interactions.
- 2) Using the 114 K/10 K $J(di)$ parameters (models $(1a,1c)_2$ and $(1a,1c)_2'$ in Figure 6), the shape of the experimental $\chi T(T)$ curve is reproduced in the whole (0–

280 K) temperature range (that is, at low-temperatures the computed $\chi T(T)$ curves distinguish between a 2D magnetic topology presenting antiferromagnetic interactions and a 3D ferromagnetic topology).

- 3) The $\chi T(T)$ curves obtained using these two models (Figure 5b) with 114 K/10 K $J(di)$ parameters are very similar, the 10 K curve with model $(1a,1c)_2'$ being nearly identical to the experimental $\chi T(T)$ data.
- 4) At 298 K and 114 K, the $\chi T(T)$ curves converge reasonably fast along the a , b , and c directions (the numerical variation between $\chi T(T)$ values among different models is always small), although none of these models fully match the experimental values (see Supporting Information Figure S1 for 298 K, and Figures S2 and S3 for 114 K).
- 5) The use of the values 0, ± 0.02 , or ± 0.07 cm⁻¹ for the $J(d6)$ parameter at 298 K has no noticeable impact on the shape of the curves (see Figure S4 in the Supporting Information).
- 6) A scaling multiplicative factor^[24] of 2.6 has to be applied to the energy levels of the 298 K Hamiltonian in order to fully match the experimental results in the 3–280 K range (Figure 6).
- 7) The scaling is 2.4 and 1.9 for the $(1a,1c)_2$ and $(1a,1c)_2'$ 3D models at 114 K (Figure 6). The smaller scaling factor required for model $(1a,1c)_2'$ suggests that it is more appropriate than model $(1a,1c)_2$ to reproduce the 3D magnetic topology of YUJNEW (Figure 5b). This is also supported by the computed $\chi T(T)$ data at 10 K, for which no scaling factor is needed when using model $(1a,1c)_2'$.

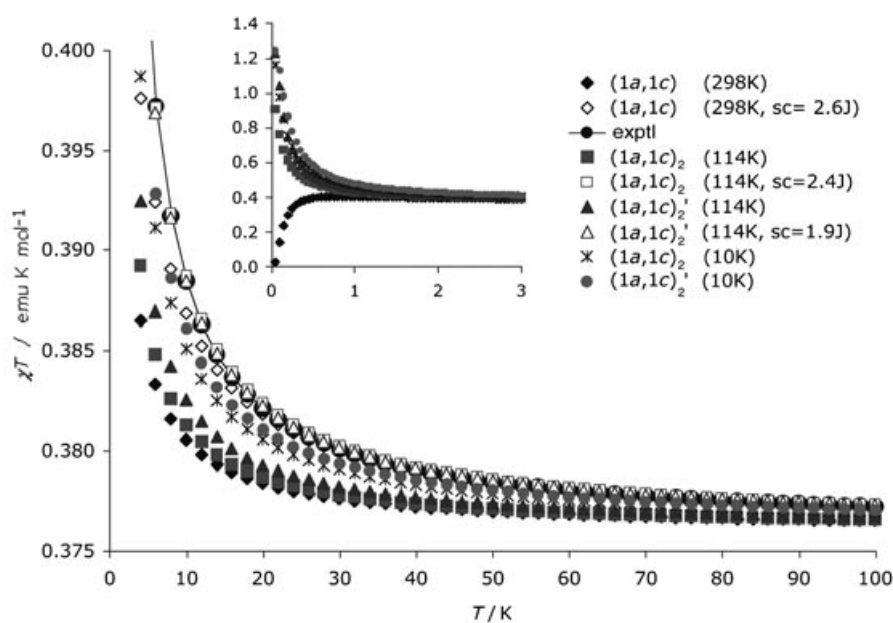


Figure 6. $\chi T(T)$ computed using $(1a,1c)$ and $(1a,1c)_2$ – $(1a,1c)_2'$ minimal magnetic models (2D and 3D models at 298 K and 114 K/10 K, respectively). See the inset on the right of the graph for an explanation of the symbols. The range of temperature shown for simulated $\chi T(T)$ data is 0–100 K (above 100 K all models converge to the same value). Inset the very low $\chi T(T)$ temperature region is also shown for all three minimal magnetic models (same symbol code applies). The experimental data are also shown. Hollow symbols represent the re-computed $\chi T(T)$ data after applying a scaling factor of 2.6 and 2.4–1.9 to the energy levels obtained using $(1a,1c)$ and $(1a,1c)_2$ – $(1a,1c)_2'$ models at 298 and 114 K, respectively.

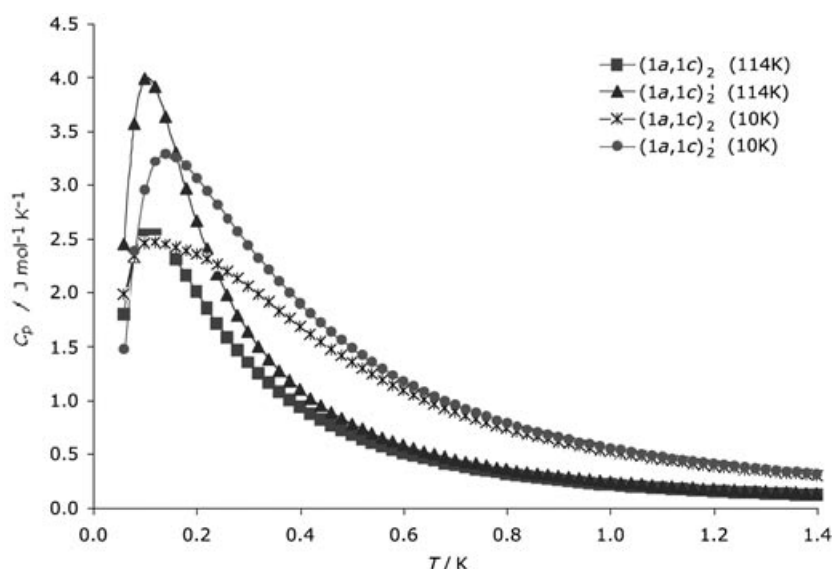


Figure 7. Simulated $C_p(T)$ data for YUNEW using the minimal $(1a,1c)_2$ and $(1a,1c)_2'$ models at 114 K/10 K (after checking these models behave ferromagnetically in the whole temperature range). See the inset on the right of the graph for an explanation of the symbols.

8) Although room-temperature crystal structures give reasonably good *qualitative* agreement with experimental $\chi T(T)$ data in many cases,^[11] the study of the magnetism of the *p*-(MeS)PhNN crystal with crystallographic data at different temperatures indicates that low-temperature crystal structures should be used in order to obtain *quantitative* agreement between computed and experimental $\chi T(T)$ data.

We finally focus on the heat capacity curve (C_p vs T , Figure 7). As we have shown the 2D minimal magnetic model $(1a,1c)$ not to be valid at low temperatures, we present only the curve computed below 3 K using the 3D minimal magnetic models $(1a,1c)_2$ and $(1a,1c)_2'$ (Figure 5b) with the 114 K and 10 K J_{AB} values. In all cases the curve is similar, presenting a maximum at approximately 0.12 K, a value that can be taken as the estimate for the computed ordering temperature. This estimate agrees very well with the experimental value of 0.20 K (obtained by *ac* susceptibility measurements in 0.18–1.0 K range).

Conclusion

By means of our first principles, bottom-up methodology we have been able to reproduce the experimental macroscopic data for the *p*-(MeS)PhNN crystal: dimensionality of the magnetic topology, shape of the magnetic susceptibility and heat capacity curves, and range of the critical temperature. These results have been obtained by using a systematic procedure that makes no a priori assumptions. This procedure also preserves the relationship between the macroscopic magnetic properties and the microscopic parameters that describe the magnetic interaction between adjacent radicals, thus connecting the macroscopic properties with the crystal

packing. This makes it possible to simulate the modifications required in the crystal packing to induce a change in macroscopic magnetic properties, which will be important for the design of new molecular magnets.

The magnetic topology of the *p*-(MeS)PhNN crystal at 298 K, 114 K and 10 K has been determined. At 298 K, it behaves as a 2D magnet within the *ac* plane, with dominant ferromagnetic interactions (+0.24 and +0.09 cm^{-1}), but also an antiferromagnetic interaction (−0.11 cm^{-1}). The interplane interactions (along the *b* axis) are found to be ferromagnetic, but are numerically negligible (+0.02 cm^{-1}). At 114 K, the magnetic topology is that of a 3D ferromagnet: in-plane J_{AB}

interactions are +0.11 and +0.07 cm^{-1} (the antiferromagnetic interaction at 298 K is now negligible, −0.02 cm^{-1}) and the only non-negligible interplane J_{AB} interaction is +0.07 cm^{-1} . At 10 K, the magnetic topology is also a 3D ferromagnet, with in-plane J_{AB} interactions +0.22 and +0.07 cm^{-1} , while the interplane J_{AB} interaction becomes +0.08 cm^{-1} . Thus, the low-temperature magnetic topology is clearly that of a bulk ferromagnet.

Using the J_{AB} values, we computed the matrix representation of the Heisenberg Hamiltonian in a finite space sufficient to represent the properties of the infinite crystal. From the energy spectrum of the Hamiltonian computed in this finite space we simulated the macroscopic magnetic susceptibility and heat capacity for *p*-(MeS)PhNN. The computed $\chi T(T)$ values reproduce qualitatively the shape of the experimental curve in the whole range of temperatures when the 3D minimal model obtained from the 114 K magnetic topology is used. However, the experimental $\chi T(T)$ curve is only quantitatively reproduced using the magnetic topology at 10 K. The heat capacity $C_p(T)$ curve shows a peak around the experimental value (0.12 K, the experimental value being 0.20 K).

All of these results indicate the importance of performing ab initio computations as part of a bottom-up strategy to analyze the magnetic properties of molecular crystals. Our results show that this strategy is particularly important in complex crystal structures, in which either a complicated interplay between ferromagnetic and antiferromagnetic interactions can exist, or in which the nature of the interactions cannot be clearly envisaged. We also found that it is essential to perform the analysis of the magnetic properties of purely organic crystals by using low-temperature crystal structures, even in the absence of crystallographic phase transitions. In this work we have thus shown that for a safe prediction/rationalization of the magnetic properties of mo-

lecular crystals one should use crystal structures determined at low-temperature, as close as possible to the transition temperature.

Acknowledgement

M.D. and J.J.N. acknowledge the Spanish “Ministerio de Ciencia y Tecnología” (# BQU2002–04587-C02–02), and the Catalan “CIRIT” (2001SGR-0044) for funding. The authors also thank CEPBA-IBM Research Institute, CEPBA, and CESCA for allocation of CPU time in their computers. M.D. thanks the Spanish “Ministerio de Ciencia y Tecnología” for the award of a “Ramón y Cajal” Fellowship at Universitat de Barcelona. This project was partly supported by EPSRC (UK) under grant GR/M86750 (ROPA).

- [1] a) “Magnetic Molecular Materials”: *NATO ASI Ser. Ser. E* **1991**, 198, whole volume; b) J. S. Miller, A. J. Epstein, *Angew. Chem.* **1994**, 106, 399; *Angew. Chem. Int. Ed. Engl.* **1994**, 33, 385; c) O. Kahn, *Molecular Magnetism*, VCH, New York, **1993**; d) “Molecular Magnetism: from Molecular Assemblies to the Devices”: *NATO ASI Ser. Ser. E* **1996**, 321, whole volume; e) *Magnetic Properties of Organic Materials* (Ed.: P. M. Lahti), Marcel Dekker, New York, **1999**; f) *Molecular Magnetism. New Magnetic Materials* (Eds.: K. Itoh, M. Kinoshita), Gordon and Breach, Amsterdam, **2000**; g) “ π -Electron Magnetism. From Molecules to Magnetic Materials”: *Struct. Bonding* **2001**, 100, whole volume; h) *Magnetism: Molecules to Materials (I–IV)* (Eds.: J. S. Miller, M. Drillon), Wiley-VCH, Weinheim, **2003**.
- [2] A. Caneschi, F. Ferraro, D. Gatteschi, A. le Lirzin, E. Rentschler, *Inorg. Chim. Acta* **1995**, 235, 159.
- [3] A. Caneschi, F. Ferraro, D. Gatteschi, A. le Lirzin, M. A. Novak, E. Rentschler, R. Sessoli, *Adv. Mater.* **1995**, 7, 476.
- [4] a) Y. Pontillon, A. Caneschi, D. Gatteschi, A. Grand, E. Ressourche, R. Sessoli, J. Schweizer, *Chem. Eur. J.* **1999**, 5, 3616; b) Y. Pontillon, A. Caneschi, D. Gatteschi, E. Ressourche, J. Schweizer, R. Sessoli, *Physica B* **1999**, 267–268, 51.
- [5] S. Pillet, M. Souhassou, Y. Pontillon, A. Caneschi, D. Gatteschi, C. Lecomte, *New J. Chem.* **2001**, 25, 131.
- [6] As we discuss in main text, these two constants J and J' cannot strictly be considered as microscopic pair interactions. Instead J and J' are an average of various microscopic fitting parameters. Notice that in their original paper,^[3] the authors used a model based on the Heisenberg Hamiltonian $\hat{H} = \sum J \hat{S}_A \cdot \hat{S}_B$ with an additional mean field correction J' to fit the experimental $\chi(T)$ data. The resulting fitting parameters were $J = -0.35$ K and $J' = -0.042$ K. As our Heisenberg Hamiltonian is expressed as $\hat{H} = -2 \sum J_{AB} \hat{S}_A \cdot \hat{S}_B$, it is appropriate to express the fitting parameters J, J' in terms of it: $J = +0.18$ K and $J' = +0.042$ K.
- [7] a) M. Deumal, C. Cirujeda, J. Veciana, J. J. Novoa, *Adv. Mater.* **1998**, 10, 1461; b) M. Deumal, C. Cirujeda, J. Veciana, J. J. Novoa, *Chem. Eur. J.* **1999**, 5, 1631.
- [8] H. M. McConnell, *J. Chem. Phys.* **1963**, 39, 1910.
- [9] M. Deumal, J. J. Novoa, M. J. Bearpark, P. Celani, M. Olivucci, M. A. Robb, *J. Phys. Chem. A* **1998**, 102, 8404.
- [10] a) J. J. Novoa, M. Deumal, *Struct. Bonding* **2001**, 100, 34; b) J. J. Novoa, M. Deumal, P. Lafuente, M. A. Robb, *Mol. Cryst. Liq. Cryst.* **1999**, 335, 603.
- [11] a) M. Deumal, M. J. Bearpark, J. J. Novoa, M. A. Robb, *J. Phys. Chem. A* **2002**, 106, 1299; b) M. Deumal, M. A. Robb, J. J. Novoa, *Polyhedron* **2003**, 22, 1935; c) M. Deumal, C. P. Landee, J. J. Novoa, M. A. Robb, M. M. Turnbull, *Polyhedron* **2003**, 22, 2235.
- [12] Notice that in previous papers^[11] we refer to the structure resulting from the connections established between magnetically non-negligible J_{AB} pair interactions as *magnetic structure*. In this paper we have re-named it as *magnetic topology* in order to avoid misunderstandings with experimental information related to polarized neutron diffraction measurements.
- [13] See for instance: a) I. Castro, M. L. Calatayud, J. Sletten, F. Lloret, J. Cano, M. Julve, G. Seitz, K. Mann, *Inorg. Chem.* **1999**, 38, 4680; b) C. Benelli, J. Cano, Y. Journaux, R. Sessoli, G. A. Solan, R. E. P. Winpenny, *Inorg. Chem.* **2001**, 40, 188.
- [14] Several alternative approaches can be used to compute J_{AB} pair interactions—see, for example: a) solid-state methods, such as CRYSTAL (R. Orlando, R. Dovesi, P. Ugliengo, C. Roetti, V. R. Saunders, *Int. J. Inorg. Mater.* **1999**, 1, 147), and b) cluster approach/dimeric computation (J. Cabrero, N. Ben Amor, C. de Graaf, F. Illas, R. Caballol *J. Phys. Chem. A* **2000**, 104, 9983; E. Ruiz, J. Cano, S. Alvarez, P. Alemany, *J. Comput. Chem.* **1999**, 20, 1391; reference [11]).
- [15] a) L. Noodleman, *J. Chem. Phys.* **1981**, 74, 5737; b) L. Noodleman, E. R. Davidson, *Chem. Phys.* **1986**, 109, 131.
- [16] a) A. D. Becke, *Phys. Rev. A* **1988**, 38, 3098; b) C. Lee, W. Yang, R. G. Parr, *Phys. Rev. B* **1988**, 37, 785; c) A. D. Becke, *J. Chem. Phys.* **1993**, 98, 5648.
- [17] R. Ditchfield, W. J. Hehre, J. A. Pople, *J. Chem. Phys.* **1971**, 54, 724.
- [18] a) E. Ruiz, P. Alemany, S. Alvarez, J. Cano, *J. Am. Chem. Soc.* **1997**, 119, 1297; b) R. Caballol, O. Castell, F. Illas, I. D. R. Moreira, J. P. Malrieu, *J. Chem. Phys.* **1997**, 101, 7860; c) M. Nishino, Y. Shigeta, T. Soda, Y. Kitagawa, T. Onishi, Y. Yoshioka, K. Yamaguchi, *Coord. Chem. Rev.* **2000**, 198, 265; d) J.-M. Mouesca, *J. Chem. Phys.* **2000**, 113, 10505; e) F. Illas, I. D. R. Moreira, C. de Graaf, V. Barone, *Theor. Chem. Acc.* **2000**, 104, 265.
- [19] M. J. Frisch, G. W. Trucks, H. B. Schlegel, P. M. W. Gill, B. G. Johnson, M. A. Robb, J. R. Cheeseman, T. Keith, G. A. Petersson, J. A. Montgomery, K. Raghavachari, M. A. Al-Laham, V. G. Zakrzewski, J. V. Ortiz, J. B. Foresman, J. Cioslowski, B. B. Stefanov, A. Nanayakkara, M. Challacombe, C. Y. Peng, P. Y. Ayala, W. Chen, M. W. Wong, J. L. Andres, E. S. Replogle, R. Gomperts, R. L. Martin, D. J. Fox, J. S. Binkley, D. J. Defrees, J. Baker, J. J. P. Stewart, M. Head-Gordon, C. Gonzalez, J. A. Pople, *Gaussian 98*, Gaussian, Inc., Pittsburgh PA, **1999**.
- [20] Refcode according to Cambridge Crystallographic Database (CCSD): a) F. H. Allen, J. E. Davies, J. J. Galloy, O. Johnson, O. Kennard, C. F. Macrae, D. G. Watson, *J. Chem. Inf. Comput. Sci.* **1991**, 31, 204; b) F. H. Allen, O. Kennard, *Chem. Des. Automation News* **1993**, 8, 31.
- [21] The theoretical value for non-interacting $S=1/2$ species is $C = 0.376$ emu K mol⁻¹. In reference [2] the Curie constant C is taken as a fitting parameter and values for C of 0.35 emu K mol⁻¹ and $\theta = 0.32$ K were obtained.
- [22] M. Deumal, P. Lafuente, F. Mota, J. J. Novoa, *Synth. Met.* **2001**, 122, 477; for atomic (Mulliken) spin populations, see Table S1 in the Supporting Information.
- [23] We have chosen such a limit to be $|0.05|$ cm⁻¹ due to the number of significant digits we have in the energy of the high and low spin states, with the cutoffs employed in the computation of the integrals and in the self-consistent process.
- [24] Scaling factors produce a uniform increase in the separations between energy levels, but not a change in their nature. They account for the small differences between the exact and DFT-computed values of J_{AB} , possible third and higher order cooperative effects, and possible errors introduced by the use of finite magnetic model spaces and room-temperature crystal structures. Here, the linear scaling factor applied over all J_{AB} parameters is $J_{AB}' = a J_{AB}$.

Received: May 18, 2004
Published online: November 5, 2004